Journal of Neurochemistry

JOURNAL OF NEUROCHEMISTRY | 2018 | 146 | 585–597

doi: 10.1111/jnc.14465

ORIGINAL ARTICLE

# Differential toxicity of TAR DNA-binding protein 43 isoforms depends on their submitochondrial localization in neuronal cells

Illari Salvatori*[1], Alberto Ferri*†[1], Silvia Scaricamazza*‡, Ilaria Giovannelli*, Alessia Serrano§, Simona Rossi¶, Nadia D'Ambrosi‡, Mauro Cozzolino*¶, Andrea Di Giulio**, Sandra Moreno**, Cristiana Valle*† and Maria Teresa Carrì*‡

*Fondazione Santa Lucia IRCCS, c/o CERC, Rome, Italy

†Institute for Cell Biology and Neurobiology, CNR, c/o CERC, Rome, Italy

‡Department of Biology, University of Rome Tor Vergata, Rome, Italy

§Institute of Anatomy and Cell Biology, Università Cattolica del Sacro Cuore, Rome, Italy

¶Institute of Translational Pharmacology, CNR, Rome, Italy

**Department of Science, LIME, University Roma Tre, Rome, Italy

**Abstract**

TAR DNA-binding protein 43 (TDP-43) is an RNA-binding protein and a major component of protein aggregates found in amyotrophic lateral sclerosis and several other neurodegenerative diseases. TDP-43 exists as a full-length protein and as two shorter forms of 25 and 35 kDa. Full-length mutant TDP-43s found in amyotrophic lateral sclerosis patients re-localize from the nucleus to the cytoplasm and in part to mitochondria, where they exert a toxic role associated with neurodegeneration. However, induction of mitochondrial damage by TDP-43 fragments is yet to be clarified. In this work, we show that the mitochondrial 35 kDa truncated form of TDP-43 is restricted to the intermembrane space, while the full-length forms also localize in the mitochondrial matrix in cultured neuronal NSC-34 cells. Interestingly, the full-length forms clearly affect mitochondrial metabolism and morphology, possibly via their ability to inhibit the expression of Complex I subunits encoded by the mitochondrial-transcribed mRNAs, while the 35 kDa form does not. In the light of the known differential contribution of the full-length and short isoforms to generate toxic aggregates, we propose that the presence of full-length TDP-43s in the matrix is a primary cause of mitochondrial damage. This in turn may cause oxidative stress inducing toxic oligomers formation, in which short TDP-43 forms play a major role.

**Keywords:** amyotrophic lateral sclerosis, Complex I, localization, mitochondria, neurodegeneration, TDP-43.

*J. Neurochem.* (2018) **146**, 585–597.

TAR DNA-binding protein 43 (TDP-43) is a major component of ubiquitinated inclusions that characterize amyotrophic lateral sclerosis (ALS) and frontotemporal lobar degeneration (FTLD) (Arai *et al.* 2006; Neumann *et al.* 2006), as well as an increasing spectrum of other neurodegenerative diseases that may be collectively considered 'TDP-43 proteinopathies' such as Alzheimer's disease

Received February 20, 2018; revised manuscript received March 20, 2018; accepted April 23, 2018.

Address correspondence and reprint requests to Maria Teresa Carrì, Department of Biology, University of Rome Tor Vergata, Via della Ricerca Scientifica, 00133 Rome, Italy. E-mail: carri@bio.uniroma2.it (or) Cristiana Valle, Institute for Cell Biology and Neurobiology, CNR, Via del Fosso di Fiorano 64, 00143 Rome, Italy. E-mail: cvalle@ibc.cnr.it

[1]These authors contributed equally to this work.

*Abbreviations used*: ALS, amyotrophic lateral sclerosis; CHCHD10, Coiled-Coil-Helix-Coiled-Coil-Helix Domain Containing 10; FL, full length; FTLD, frontotemporal lobar degeneration; IMM, inner mitochondrial membrane; IMS, inner mitochondrial space; MnSOD, superoxide dismutase 2; Mtfr-1, mitochondrial fission regulator-1; ND3 and ND6, NADH-ubiquinone oxidoreductase chain 3 and 6; NDUB5, NADH ubiquinone oxidoreductase subunit B5; OCR, oxygen consumption rate; OMM, outer mitochondrial membrane; RRID, research resource identifier; RRM, RNA-recognition motifs; SOD1, superoxide dismutase 1; TDP-43, TAR DNA-binding protein 43.

 

(Chen-Plotkin *et al.* 2010), Parkinson's disease (Lin and Dickson 2008), Huntington's disease (Schwab *et al.* 2008), hippocampal sclerosis (Amador-Ortiz *et al.* 2007) and dementia with Lewy bodies (Lin and Dickson 2008).

TDP-43 is an RNA-binding protein with two RNA-recognition motifs named RNA-recognition motifs 1 and 2 (RRM1 and RRM2). Under physiological conditions, TDP-43 is mainly located in the nucleus, where it acts as a regulator of microRNA biogenesis, RNA splicing and RNA transport. Under stress conditions, TDP-43 is recruited to stress granules, the cytoplasmic site of storage of RNAs where the bulk of mRNAs are translationally repressed in these conditions. Whether the typical neuronal loss observed in ALS and FTLD is dependent upon the nuclear depletion of TDP-43 or upon a new toxic function acquired by the protein in its cytoplasmic localization is still debated. Previous work provided evidence that the cytoplasmic mislocalization of TDP-43 is sufficient to evoke neurodegeneration (Barmada *et al.* 2010). More recently, in addition to TDP-43 cytoplasmic localization, its aberrant association with mitochondria and a role for the protein in mitochondrial toxicity are emerging. In yeast, human wild-type TDP-43 localizes in mitochondria and affects respiratory capacity and functionality of the electron transport chain (Braun *et al.* 2011). Moreover, human wild-type and ALS-linked mutant TDP-43s localize to mitochondria of murine motor neurons, where they activate mitophagy and alter mitochondrial functions (Lu *et al.* 2012).

An altered distribution of mitochondria in motor neurons of TDP-43 transgenic mice has been described (Shan *et al.* 2010), while disturbed calcium handling because of TDP-43-mediated disruption of ER-mitochondria interaction has been observed in neuronal cell lines (Stoica *et al.* 2014). In addition, ALS-related TDP-43 mutations enhance the association of this protein with mitochondria (Wang *et al.* 2013, 2016). In this compartment, mutant TDP-43s (and, to a lesser extent, wild type TDP-43) impair specifically the assembly of Complex I by inhibiting the translation of NADH-ubiquinone oxidoreductase chain 3 (ND3) and NADH-ubiquinone oxidoreductase chain 6 (ND6) through the direct interaction with their mitochondrial mRNAs (Wang *et al.* 2016). According to Wang and colleagues, the entry of TDP-43 into mitochondria is driven by three internal protein motifs enriched in hydrophobic amino acids, named M1, M3 and M5, whose deletion inhibits mitochondrial import of exogenously expressed TDP-43 (Wang *et al.* 2016).

TDP-43 exists in various isoforms, generated by caspases that recognize endogenous cleavage sites in the protein, producing two C-terminal fragments, a 25 kDa and a 35 kDa fragment, which are found in neurons of patients affected by either ALS or FTLD (Neumann *et al.* 2006; Zhang *et al.* 2007), or by other neurodegenerative diseases (Tremblay *et al.* 2011). Differently from the 25 kDa fragment, the 35 kDa TDP-43 (also called T86 TDP-43) retains both RRM1 and RRM2 sequences responsible for the interaction with RNA, thus maintaining the ability to regulate RNA maturation (Kitamura *et al.* 2016). However, this truncated form has a defective nuclear localization signal and accumulates in the cytoplasm where it is highly prone to form aggregates (Bozzo *et al.* 2016). This fragment also lacks the M1 sequence, which reportedly drives the mitochondrial localization of TDP-43 (Wang *et al.* 2016), but retains the other M3 and M5 putative signals. To date, the role of 25 and 35 kDa TDP-43 forms in neuronal toxicity is still unclear and scanty data on their role in the induction of mitochondrial damage are available so far.

In this study, using a murine motor neuron cell model, expressing either two different full-length ALS-mutant TDP-43s [Q331K TDP-43 and M337V TDP-43, later referred as full length (FLs)] or the 35 kDa pathological truncated form of TDP-43 (T86 TDP-43), we investigated the subcellular distribution of these proteins and the respective mitochondrial alterations associated with their localization.

## Materials and methods

### Antibodies and reagents

The antibodies used in this study were: anti-Myc clone 9E10 monoclonal [Sigma-Aldrich, Milano, Italy, Cat# B7554, research resource identifier (RRID):AB_439695, 1 : 5000 in western blot (WB), 1 : 700 in immunofluorescence (IF), 1 : 1000 in RNA immunoprecipitation (RIP)], anti-TARDBP rabbit polyclonal (Proteintech Group, United Kingdom, Cat# 12892-1-AP, RRID: AB_2200505, WB: 1 : 1000), anti-superoxide dismutase 1 rabbit polyclonal (Enzo Life Sciences, Roma, Italy, Cat# SOD-100D, RRID:AB_2193763, WB: 1 : 2000), anti-VDAC mouse monoclonal (Santa Cruz Biotechnology, Inc., Heidelberg Germany, Cat# sc-8829, RRID:AB_2214801, WB 1 : 5000), anti-β-Actin (Santa Cruz Biotechnology, Cat# sc-47778 horseradish peroxidase, RRID: AB_2714189, WB 1 : 5000), anti-GAPDH mouse monoclonal (Santa Cruz Biotechnology, Cat# sc-166545, RRID:AB_2107299 WB 1 : 5000), anti-superoxide dismutase 2 rabbit polyclonal (Enzo Life Sciences, Cat# ALX-804-265-C100, RRID:AB_2051889, WB: 1 : 1000, IF: 1 : 200), anti-HDAC1 rabbit polyclonal (Santa Cruz Biotechnology, Cat# sc-7872, RRID:AB_2279709, WB 1 : 1000), anti-Hsp60 mouse monoclonal (Thermo Fisher Scientific, Monza MB, Italy, Cat# MA3-013, RRID: AB_325461, WB: 1 : 1000), anti-TOM20 rabbit polyclonal (Santa Cruz Biotechnology, Cat# sc-11415, RRID: AB_2207533, WB: 1 : 1000), anti-COX4 mouse polyclonal (Santa Cruz Biotechnology, Cat# sc-58348, RRID: AB_2229944, WB: 1 : 1000), anti-MT-ND3-N-terminal rabbit polyclonal (Abcam, Cambridge, UK, Cat# ab192306, WB: 1 : 1000), anti-ND6 rabbit polyclonal (Santa Cruz Biotechnology, Cat# sc-20667, RRID: AB_2282522, WB: 1 : 1000), anti-NADH ubiquinone oxidoreductase subunit B5 mouse polyclonal (Abcam, Cat# ab96228, WB: 1 : 1000). Anti-rabbit (Cat# 1706515, WB: 1 : 1000) and anti-mouse (Cat# 1706516, WB: 1 : 1000) IgG peroxidase-conjugated secondary antibodies were from Bio-Rad Laboratories, Hercules, CA, USA. Reagents, unless differently specified, were obtained from Sigma-Aldrich.

### Plasmids and cell lines

Plasmids containing sequences coding for N-terminal 5× Myc-tagged human wild-type (Accession no. Q13148), Q331K, M337V and T86 TDP-43 are shown in Figure S1 and were obtained as previously described (Bozzo *et al.* 2016). Mouse motoneuronal cell line NSC34 stably transfected with the pTetON plasmid coding for the reverse tetracycline controlled transactivator (NSC34/pTetON clone 7 and reported in this manuscript as NSC-34 untrasfected cells) was described elsewhere (Ferri *et al.* 2006).

Cells were grown in Dulbecco's modified Eagle's/F-12 medium supplemented with 10% fetal bovine serum (tetracycline free, Euroclone), at 37°C in an atmosphere of 5% $CO_2$ in air. Transfection for transient and stable expression of each vector (1.5 μg of DNA/3 × $10^5$ cells) was obtained with Lipofectamine (Invitrogen, Carlsbad, CA, USA, Cat# 1832-012) and Plus reagent (Invitrogen, Cat# 11514-015) according to manufacturer's instruction. For transient expression, after 3 h incubation with transfection reagents, cells were shifted to normal growth medium. For stable expression, after 3 weeks of selection with 400 μg/mL G418 (Gibco, Rockville, MD, USA, Cat# 10131-027) single clones were isolated and screened by western blot. The lines with higher expression were chosen for further experiments.

Induction of TDP-43 expression, in transiently and stably transfected cells, was obtained by adding to the culture medium 1 μg/mL doxycycline (Sigma-Aldrich, Cat# d3447) for 48 h.

### Subcellular fractionation and mitochondrial purification

Nuclear, cytosolic and mitochondrial extracts were prepared from NSC-34 derived cell lines homogenized in a buffer containing 210 mM mannitol, 70 mM sucrose, 1 mM EDTA and 10 mM HEPES KOH at pH 7.5 in a potter homogenizer with a Teflon piston, following the isolation procedure described by Frezza (Frezza *et al.* 2007).

Submitochondrial compartment fractionation was performed according to Wang (Wang *et al.* 2016) with some modification. Briefly, isolated pure mitochondria were washed with 50 mM KCl to avoid any spurious association of cytosolic proteins with mitochondria, resuspended in isolation medium (225 mM mannitol, 75 mM sucrose, 0.1 mM EGTA, 20 mM HEPES, digitonin 1.5 mg digitonin/mL; pH 7.4) and stirred gently on ice for 15 min. For each cell line, protein extracts from the various cell compartments (cytosol, nucleus, and mitochondria) were resuspended in RIPA buffer (50 mM Tris–HCl pH 7.4, 0.5% Triton X-100, 0.25% Na-deoxycholate, 0.1% sodium dodecyl sulfate (SDS), 250 mM NaCl, 1 mM EDTA and 5 mM $MgCl_2$) containing a protease inhibitor mixture (Sigma-Aldrich, Cat# P8340) and quantified by spectrophotometric determination with the Bradford protein assay (Bio-Rad, Cat# 5000006). Total cell protein weight was calculated by summing up data recorded for the individual cell compartments; this value was set as 100% and the percentages of each cell compartment were subsequently assigned.

Protein extracts were brought to a concentration of 1 μg/μL and 20 μg of each sample was subjected to standard electrophoresis and western blot analysis using an anti-Myc antibody. Numerical values obtained by densitometric analysis with the ImageJ software (National Institutes of Health, Bethesda, MD, USA; http://imagej.nih.gov/ij/) were multiplied by the percentage of the respective cellular compartment (assigned as above) and these values were expressed as percentages of the total, set as 100%. To avoid inaccuracies in the attribution and comparison of numerical values obtained through densitometric analysis, all fractions were loaded onto a single gel and then processed as a single filter. This procedure prevented errors because of different exposure times.

### Cell and mitochondria lysis

Total mitochondria and total cell lysates were obtained by re-suspending purified mitochondria and intact cells in RIPA buffer as above, containing a protease inhibitor mixture (Sigma-Aldrich, Cat# P8340). A clear supernatant was obtained by centrifugation of lysates at 17 000 *g* for 20 min. Protein content was determined using the Bradford protein assay.

### Electrophoresis and western blotting

Protein samples were separated by SDS–polyacrylamide gel electrophoresis and transferred to nitrocellulose membranes (Perkin Elmer, Cat# NBA085B). Membranes were blocked for 1 h in Tris-buffered saline solution with 0.1% Tween-20 (TBS-T) containing 5% non-fat dry milk, and then incubated for 2 h at room temperature or overnight at 4°C with indicated primary antibodies, diluted in TBS-T containing 2% non-fat dry milk. After rinsing with TBS-T solution, membranes were incubated for 1 h with the appropriate peroxidase-conjugated secondary antibody diluted in TBS-T containing 1% non-fat dry milk, then washed and developed using the enhanced chemiluminescence detection system (Roche Molecular Diagnostics, CA, USA, Cat# n11500694001). Densitometric analyses were performed using ImageJ software program (U. S. National Institutes of Health, Bethesda, Maryland, USA, https://imagej.nih.gov/ij/, 1997-2016). The apparent molecular weight of proteins was determined by calibrating the blots with pre-stained molecular weight markers (Bio-Rad Laboratories, Cat# 161-0394).

### RNA immunoprecipitation and RT-PCR/Real-Time PCR

Isolated mitochondria were lysed in Lysis Buffer (20 mM NaCl, 250 mM NaCl, 1.5 mM MgCl2, 0.2% Triton X-100; pH 8.0) containing 0.2 U/μL RNAsin (Promega, Madison, WI, USA, Cat# N2111) and protease inhibitors cocktail (Sigma-Aldrich, Cat# P8340). Equal amounts of mitochondrial extracts of NSC-34 cell lines were incubated at 4°C for 2 h with protein G-agarose beads (Roche, Cat# 11719416001) conjugated with primary anti-Myc clone 9E10 antibody. Mouse IgGs (Santa-Cruz Biotechnology, Cat# sc-2025) were used as a negative control. After three washes with 20 mM Tris HCl pH 8.0, 50 mM NaCl and 1.5 mM $MgCl_2$, immuno-complexes were resuspended in RNA Elution Buffer (0.2 M NaOAc pH 5.0, 0.2% SDS, 1 mM EDTA) and *in vitro*-transcribed with Super Script III First Strand kit (Invitrogen, Cat# 18080051) using random primers. BC200 RNA was added as internal retro-transcription efficiency control and total mitochondrial RNA was analysed as an internal standard. qRT-PCR reactions were performed with the Light Cycler 480 SYBR Green System (Roche, Cat# 04887352001) with appropriate oligonucleotides pairs (Table S1). Cp values were calculated using the 'second derivative max' algorithm of the Lightcycler software. Immunoprecipitated mRNA quantities were calculated from Cp values using experimentally determined amplification efficiencies, and then normalized for the internal control BC200 and for the total amount of mRNA obtained from isolated mitochondrial lysates used for the respective

immunoprecipitation. To evaluate total ND3 and ND6 mRNA expression in NSC-34 cell lines, standard qRT-PCR reactions were performed and Actin and GAPDH were measured as control housekeeping genes.

### Immunofluorescence analysis

Cell cultures were grown on poly-L-lysine-coated glass slides, fixed in 4% paraformaldehyde for 10 min at 25°C, subsequently permeabilized with 0.1% Triton X-100 for 8 min and washed in phosphate-buffered saline (PBS). Samples were saturated for 30 min with 2% horse serum in PBS and incubated for 2 h at 25°C with primary antibodies, followed by Alexa Fluor 488 (Invitrogen, Cat# A11017, 1 : 300) anti-mouse goat antibodies and Cy3 anti-rabbit antibody [Jackson Immuno-Research Laboratories, West Grove, PA, USA, Cat# 65119, 1 : 300)]. After rinsing in PBS, the cells were counterstained with 1 μg/mL of Hoechst 33342 and examined using a Confocal Zeiss LSM 510 laser-scanning microscope. Fluorescence images were processed using ZEN 2009 (Carl-Zeiss-Straße, Oberkochen, Germany) and Adobe Photoshop software.

### Electron microscopic analysis

For ultrastructural analysis, cells were plated in a Chamber Slide™ system and fixed in 0.5% glutaraldehyde and 2% paraformaldehyde, in 0.1 M cacodylate buffer, pH 7.4 for 1 h, then post fixed in 1% osmium tetroxide in the same buffer for 45 min, in the dark. Samples were washed for 30 min and contrasted *en bloc* with 1% uranyl acetate in the dark, then gradually dehydrated in ethanol. All the steps of the above procedure were performed at 4°C. Cells were infiltrated with a mixture of ethanol and Epoxy Embedding Medium (Sigma-Aldrich™, Cat# 45359-1EA-F), then embedded in the same resin, allowing specimens to polymerize at 60°C, for 3 days. Samples were then analysed by a Focused Ion Beam/Scanning electron microscope (Dualbeam FIB/SEM Helios Nanolab, FEI, Hillsboro, OR, USA). Resin-embedded cells were mounted on stubs using a self-adhesive carbon disk and gold sputtered by an Emithech K550. Regions of interest were cross-sectioned by the focused gallium ion beam of the FIB/SEM, operated at 30 kV and 6.5 nA. Pictures of cross sections were acquired at a working distance of 2 mm using backscattered electrons and a through-the-lens (TLD) detector in immersion mode with an operating voltage of 2 kV and an applied current of 0.17 Na. Images were composed in an Adobe Photoshop CC format.

### Measurement of mitochondrial oxygen consumption

Seahorse XF96e Analyzer (Seahorse Bioscience-Agilent, Santa Clara CA, USA) was used to measure the oxygen consumption rate (OCR) of the cells. The experiments were performed with the Stimulus XF (Seahorse Bioscience) Stress Test Kit according to the manufacturer's instructions. Briefly, 20 000 NSC-34 cells were pre-treated with doxycycline for 48 h and seeded on micro-lysine-coated XF96 microplates in 200 μL Dulbecco's modified Eagle's medium 10% fetal bovine serum with doxycycline. To perform the Cell Mito Stress Test, medium was replaced with XF Base supplemented with 1 mM pyruvate, 2 mM glutamine and 10 mM glucose, and cells were incubated in a $CO_2$-free incubator at 37°C for 45 min.

### Spectrophotometric assays

The activity of respiratory chain complexes (Complex II/III, IV) was evaluated in mitochondria isolated from NSC-34 cell lines according to Ferri (Ferri *et al.* 2006), with some modifications. Briefly, cell lines were sonicated (UP200S Ultrasound Technology, Hielscher, Teltow, Germany, 20% Amplitude, 0.5 cycles for 30 s), and the reduction or oxidation of specific substrates was recorded by spectrophotometric measures. In particular, Complex I activity was performed by monitoring the oxidation of NADH at 340 nm at 30°C in a 1 mL quartz cuvette containing 25 mM potassium phosphate pH 7.4, 5 mM $MgCl_2$, 5 mg/mL bovine serum albumin, 1 mg/mL Antimycin A, 65 μM decylubiquinone, 130 μM NADH and 80 μg of total mitochondrial protein. Spectrophotometric determination of Citrate Synthase activity was measured according to Ferri (Ferri *et al.* 2006).

### Statistical analysis

We used Prism software (GraphPad Software, Inc. La Jolla, CA, USA) to check statistical significance. The results are presented as means ± SD of $n \geq 3$ independent experiments. Statistical evaluation was conducted by a simple Student's *t*-test, and values significantly different from the relative control are indicated with an asterisk when $p < 0.05$ and with two asterisks when $p < 0.01$. Statistical analysis of experiments containing more than two-group comparison was performed by the one-way analysis of variance (ANOVA) and Tukey's multiple comparison tests. Values significantly different from the relative control are indicated with a hashtag when $p < 0.05$ and with two hashtags when $p < 0.01$.

### Statements

This study was not pre-registered and no institutional approval was required. For this study, we did not perform blinding procedures. NSC-34 cells used in this study are not listed as a commonly misidentified cell line by the International Cell Line Authentication Committee. No randomization methods were employed for this study. The authors declare that they have no conflict of interest.

## Results

### T86 TDP-43 has a higher propensity to accumulate into mitochondria than full-length TDP-43 forms

Mitochondrial localization of TDP-43 was observed for the first time by Sasaki (Sasaki *et al.* 2010) in patients and subsequently confirmed by others in studies on cellular and animal models (Hong *et al.* 2012; Wang *et al.* 2016, 2017). Two recent elegant papers by Wang (Wang *et al.* 2016, 2017) reported that the elimination of the putative mitochondrial localization sequence M1 is sufficient to inhibit the entry of TDP-43 into the mitochondrial matrix and consequently its neuronal toxicity. Data about the localization of T86 TDP-43 into mitochondria and its related toxicity come solely from Hong and collaborators (Hong *et al.* 2012). The authors described the mitochondrial localization of FL and truncated TDP-43 forms and observed activation of autophagy by changes in LC3-II and p62.

In order to clarify the differences between T86 TDP-43 and the mutant FL TDP-43s in mediating mitochondrial damage, we used mouse motor neuron-like NSC-34 cells stably transfected with plasmids coding for the inducible

expression of two FL ALS-mutant TDP-43s (Q331K TDP-43 and M337V TDP-43) and the truncated form T86 TDP-43, provided with a 5× Myc N-terminal tag (Figure S1). Protein expression was confirmed by western blot analysis using anti-TDP-43 and anti-Myc antibodies (Figure S2a). As previously described (Bozzo *et al.* 2016), the N-terminal Myc-tag does not alter TDP-43 properties and intracellular/subcellular distribution (not shown). However, in agreement with Ayala *et al.* (2011), we observed a weak reduction in endogenous TDP-43 expression when the FL forms were expressed. This reduction, despite the presence of the RRM1 and C-terminus domains, was not observed when T86 was expressed (Figure S2a).

To evaluate the subcellular distribution of the proteins, we used a well-established fractionation protocol (Valle *et al.* 2014; Salvatori *et al.* 2017). As shown in Fig. 1(a), FLs predominantly localize in the nucleus, while T86 TDP-43 is mainly cytoplasmic, because the nuclear localization signal is partially deleted as previously reported (Liu-Yesucevitz *et al.* 2010; Bozzo *et al.* 2016). Moreover, FLs and even more consistently T86 TDP-43 have also a not negligible mitochondrial component (Fig. 1a). From an extrapolation in which we combined data obtained from western blot densitometric analysis and quantification of protein extract fractions (from cytoplasm, nucleus and mitochondria respectively) it was possible to estimate that up to 13% of T86 TDP-43 is localized at the mitochondrial level, whereas for FLs this percentage does not exceed 6% (Fig. 1b).

Furthermore, we transiently transfected NSC-34 parental cell line with plasmids coding for wild-type TDP-43 and ALS-mutant TDP-43s. This strategy allowed us to obtain a comparable expression level of the different forms of TDP-43 among NSC-34-derived cell lines (Figure S2b), a condition that is not obtained in several NSC-34-derived cell lines stably expressing wild-type TDP-43 (Figure S2a and c).

In this experimental condition, T86 again showed an increased propensity to associate with mitochondria, while wild-type TDP-43 behaved similarly to mutant FL TDP-43s (Figure S3a).

Immunofluorescence analysis confirmed these results, showing that FLs are mainly nuclear, whereas T86 TDP-43 is detected as a diffuse staining in the cytoplasm (Fig. 1c–e). Moreover, both FLs and, to a higher extent, T86 TDP-43 show a clear co-localization with a mitochondrial marker. It should be noted that under this standard growth conditions

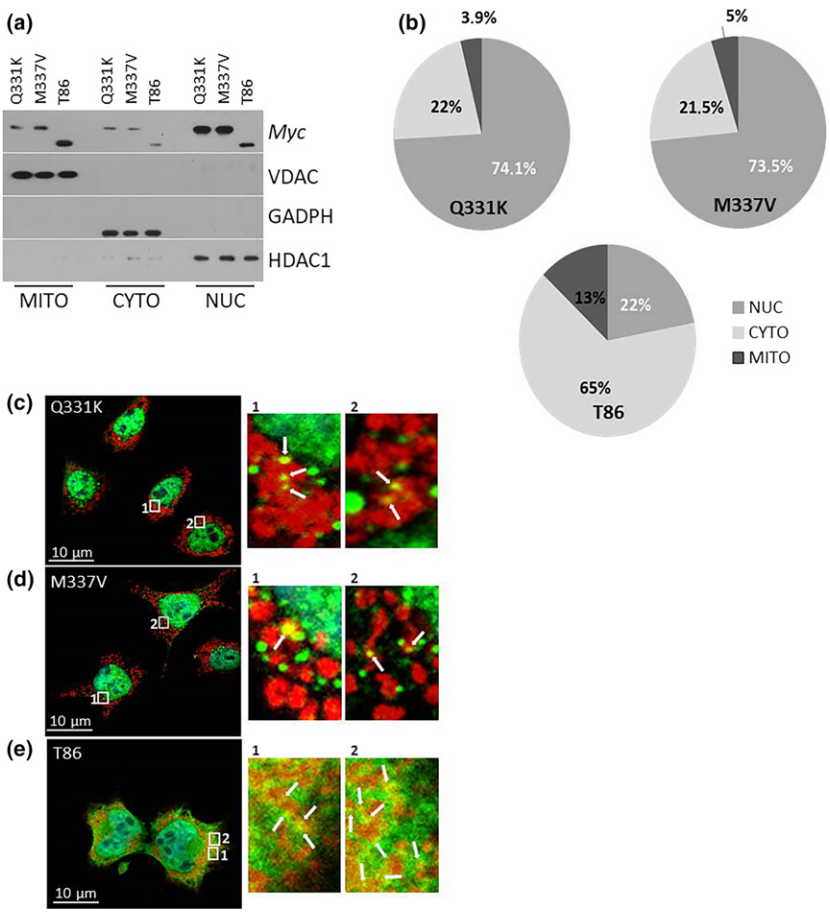


**Fig. 1** Both full-length (FL) and T86 TAR DNA-binding protein 43 (TDP-43)s localize in mitochondria. (a) Western blot analysis of nuclear (NUC), cytosolic (CYTO) and mitochondrial (MITO) protein extract obtained from NSC-34 cells stably transfected for expression of FL (Q331K and M337V) and T86 TDP-43s using anti-Myc antibody. Fractions were controlled for the presence of the nuclear marker HDAC1, the cytosolic marker GADPH and the mitochondrial marker VDAC. A representative immunoblot, out of $n = 4$ different experiments, is shown. (b) Schematic representation of an extrapolation of combined data obtained from western blot densitometric analysis, as in (a), and spectrophotometric quantification of protein extract fractions. Values are reported as the percentage of the total cellular protein extract considered 100%. (c, d, e) Immunofluorescence analysis on NSC-34 cells stably transfected for expression of FL (Q331K and M337V) and T86 TDP-43s using anti-Myc (green) and anti-MnSOD (red) antibodies. Panels show typical images observed in $n = 3$ independent experiments. Scale bar: 10 µm.

only a small fraction of TDP-43 is seen in cytoplasmic protein aggregates, in agreement with previous observations that (at least in cultured cell models) oxidative conditions are needed to induce the formation of aggregates (Bozzo *et al.* 2016 and references therein).

### Full-Length TDP-43s exert greater deleterious effects on mitochondrial functionality and morphology than T86 TDP-43

To investigate whether the accumulation of T86 TDP-43 into mitochondria correlates with alterations in mitochondrial functionality, we performed a Mito Stress Test using the Seahorse® XFe Technologies that allow the analysis of a wide panel of mitochondrial bioenergetic parameters through the real-time measurement of OCR in live cultured cells.

This experimental approach allowed us to evaluate the differences in the energy profile between untransfected and stably transfected NSC-34 cells expressing FL and T86 TDP-43s (Fig. 2a). Data analysis showed a significant difference in basal respiration between cells expressing FL TDP-43s and control NSC-34 cells, whereas basal respiration is not affected in cells expressing T86 TDP-43 (Fig. 2b).

We inferred the ATP production, analysing the difference between the basal oxygen consumption and values measured after oligomycin injection. Cells expressing FL TDP-43s show a significant drop in ATP production that, conversely, is unaffected in cell line expressing T86 TDP-43 (Fig. 2c). The addition of FCCP, dissipating the protonic gradient, maximizes the electron flow through the mitochondrial transport chain and increases oxygen consumption. The following OCR increase measures the maximal respiration, which indicates the efficiency of the electron flow. As reported in Fig. 2(d), cells expressing FL TDP-43s have a markedly reduced maximal respiration, while cells

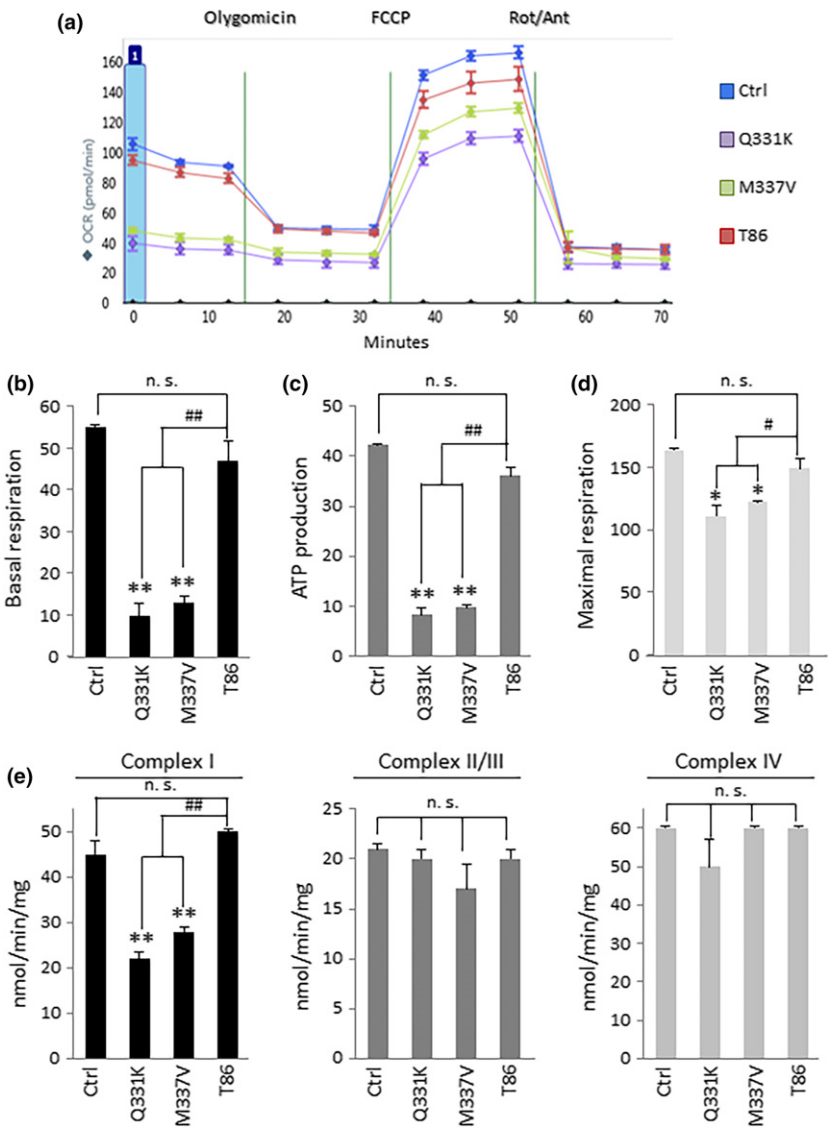


**Fig. 2** Full-length (FL) TAR DNA-binding protein 43 (TDP-43)s have detrimental effects on mitochondrial metabolism and functionality. (a) Mitochondrial stress test profile measuring oxygen consumption rate (OCR) in viable NSC-34 cells untransfected (Ctrl) and stably transfected for expression of FL (Q331K and M337V) and T86 TDP-43s. One representative experiment out of four and with each sample in sixtuplicate, is shown. (b–d) Individual parameters for basal respiration, ATP production and maximal respiration. Each data point represents an OCR measurement. Data are shown as mean ± SD. Values significantly different from relative control (Ctrl) are indicated with $*p < 0.05$ and $**p < 0.01$. Values significantly different from T86 with $\#p < 0.05$ and $\#\#p < 0.01$. n.s. indicates values that do not differ significantly. (e) Respiratory electron transport chain activity (Complexes I-IV) in isolated mitochondria from NSC-34 cells untransfected (Ctrl) and stably transfected for the expression of FL (mutant Q331K and M337V) and T86 TDP-43s. Values are expressed as nmol/min/mg protein, normalized with citrate synthase activity and are reported as mean ± SD from three independent experiments with each sample in quadruplicate. Values significantly different are reported as in (b, c and d).

expressing T86 TDP-43 have values closer to those of untransfected control cells. Finally, the injection of Rotenone and Antimycin A allows to measure the non-mitochondrial respiration and the 'loss of protons', defined as basal cellular respiration not coupled with ATP production. As shown in Fig. 2(a), there are no significant differences in non-mitochondrial respiration between the different cell lines. These data suggest that only FL TDP-43s have a noteworthy detrimental effect on mitochondrial metabolism. We performed the same Mito Stress Test on NSC-34 cells transiently transfected for the expression of wild-type TDP-43, mutant FLs and T86; wild type TDP-43 induces mitochondrial dysfunctions similar to that observed in cell lines expressing mutant FL TDP-43s, while again cells expressing T86 TDP-43 have values closer to those of untransfected control cells (Figure S3b).

In order to evaluate whether such impairment of mitochondrial functionality can be attributed to the dysfunction of a specific complex of the electron transport chain, we performed a spectrophotometric analysis of the activity of electron transport chain complexes. As shown in Fig. 2(e), the expression of FLs specifically impairs the activity of Complex I, while the expression of T86 TDP-43 does not. Finally, to evaluate whether the observed mitochondrial dysfunctions are accompanied by abnormal mitochondrial morphology, we also performed ultrastructural analysis on cell lines expressing FL and T86 TDP-43s, taking advantage of FIB/SEM technology (Fig. 3). Compared with controls (Fig. 3a and b), where mitochondria display regular membrane compartmentalization, with recognizable inner mitochondrial membrane (IMM) and outer mitochondrial membrane, cells expressing Q331K (Fig. 3c and d) show profoundly altered mitochondrial morphological features. These include abnormal enlargement of IMS, accompanied by derangement of IMM, with barely identified cristae. When present, the latter appear highly irregular, collapsed or

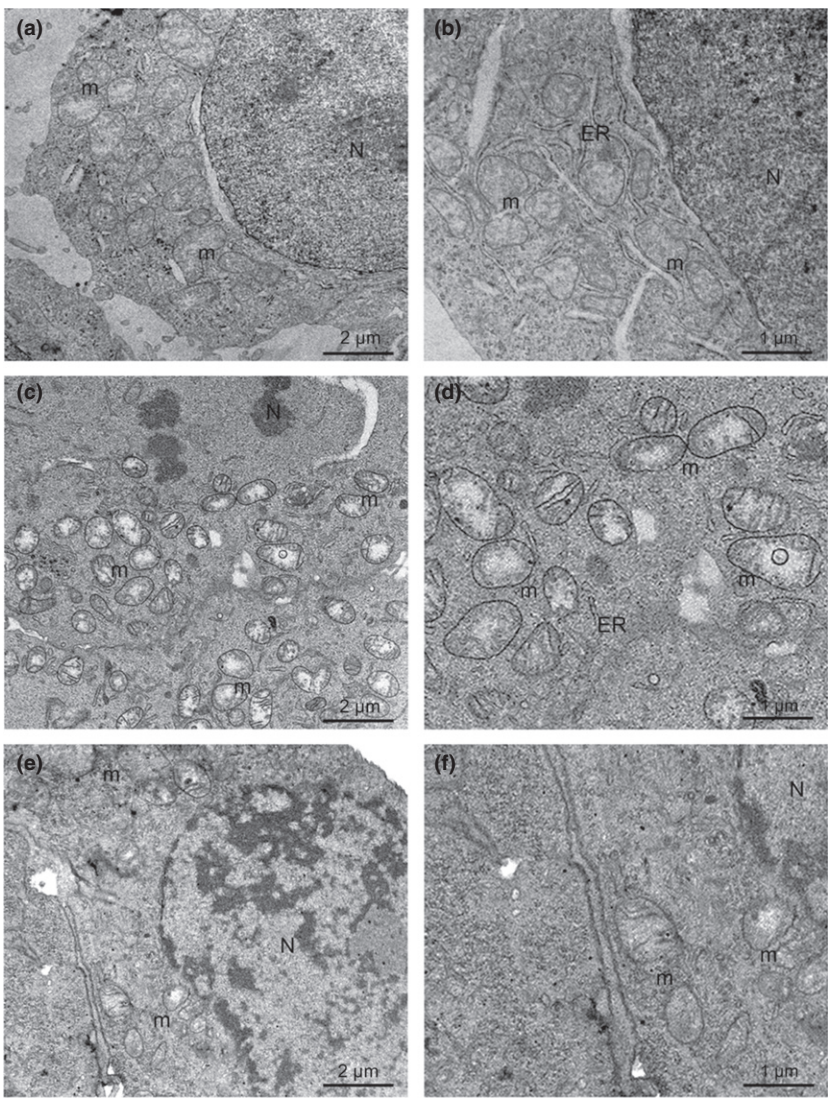


**Fig. 3** FIB/SEM ultrastructural analysis reveals dramatic mitochondrial alterations in cells expressing full-length TAR DNA-binding protein 43 (TDP-43), and milder changes in cells expressing T86 TDP-43. (a and b) Untransfected cells showing regular ultrastructural features of mitochondria. (c and d) Cells expressing Q331K TDP-43, with diffusely abnormal mitochondrial morphology. (e and f) Cells expressing T86 TDP-43, displaying mostly regular membrane compartmentalization of mitochondria with readily recognizable *cristae*. Few organelles show enlarged IMS. N, nucleus; m, mitochondria; ER, endoplasmic reticulum.

roundly shaped. Differently from the dramatic changes observed in cells expressing FL TDP-43s, milder alterations are detected in lines transfected with the T86 form (Fig. 3e and f). Indeed, few mitochondria in these cells show signs of morphological alterations, while most organelles display a preserved ultrastructure, with readily recognized cristae and normally electron-dense inner matrix compared to mitochondria from cells expressing FL TDP-43 (Figure S4).

Taken together, these results surprisingly suggest that TDP-43 mitochondrial toxicity does not depend on the amount of protein accumulated in these organelles but rather by specific mitochondrial TDP-43 forms.

### Mitochondrial accumulation of T86 TDP-43 is restricted to the IMS and this constraint hinders the binding with mRNAs localized into the matrix

Recently, it was reported that both wild-type and mutant TDP-43s co-purify with the IMM fraction of mitochondria (Wang *et al.* 2016). This localization takes place as FL TDP-43s bind mitochondria-transcribed mRNAs coding for the Complex I subunits ND3 and ND6, inhibiting their translation on ribosomes docked on the matrix facing of the IMM.

We therefore wondered if the inability of T86 TDP-43 to induce mitochondrial damage, despite its strong mitochondrial accumulation, could be attributed to a specific submitochondrial localization.

To clarify this point, we separated the various mitochondrial compartments (outer mitochondrial membrane, IMS, IMM, Matrix) to define the sublocalization of FL and T86

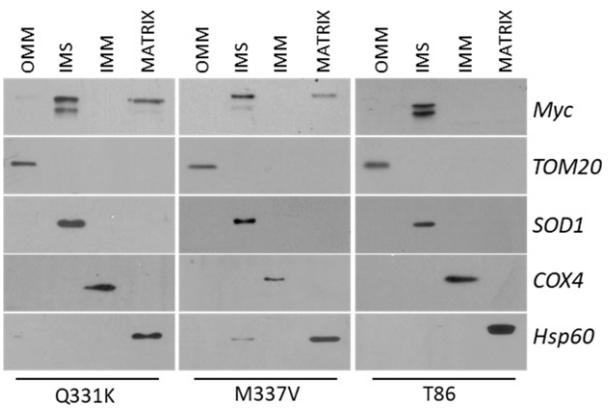


**Fig. 4** Full-length (FL) and T86 TAR DNA-binding protein 43s (TDP-43) are predominantly located in the mitochondrial intermembrane space, but part of FL TDP-43s are also found in the matrix. Western blot analysis using an anti-Myc antibody on submitochondrial fractions from isolated mitochondria obtained from NSC-34 cells untransfected (Ctrl) and stably transfected for expression of FL (Q331K and M337V) and T86 TDP-43s. A representative immunoblot, out of three experiments, is shown. Outer mitochondrial membrane (OMM), intermembrane mitochondrial space (IMS), inner mitochondrial membrane (IMM) and matrix (MATRIX) were controlled for the presence of compartment-specific markers using antibodies against TOM20, SOD1, COX4 and Hps60 respectively.

TDP-43s within the mitochondria. As shown in Fig. 4, in NSC-34 cells the localization of T86 TDP-43 is restricted to the IMS, while the FL TDP-43s are present in both the IMS and the matrix. Interestingly IMS-localized TDP-43s (and to a lesser extent matrix-localized TDP-43) appear as a double band in western blot, with the two bands having variable relative intensity. This may be attributed to differential post-translational modifications as described by Buratti (2017).

These results prompted us to examine the expression level of the subunits ND3 and ND6 of Complex I in our cell lines. As shown in Fig. 5, western blot analysis indicates that the over-expression of FL TDP-43s induces a marked reduction in the protein levels of ND3 and ND6. Differently, the levels of these proteins are not affected by the expression of T86 TDP-43. We did not observe changes in the protein level of NADH ubiquinone oxidoreductase subunit B5, a Complex I subunit encoded by the nuclear genome, in any of the conditions analysed (Fig. 5a). These data suggest that FL TDP-43s specifically inhibit the expression of subunits of Complex I encoded by the mitochondrial-transcribed mRNAs.

The transient expression of wild-type TDP-43 in NSC-34 cells induces a reduction in the ND3 and ND6 protein levels similar to that observed in NSC-34 cells transiently expressing the FL mutant forms (Figure S3c).

To corroborate the evidence of a different functional behaviour of the short and long TDP-43 forms in relation to their different mitochondrial sublocalization, we performed mRNA-IP experiments. This experiment allowed us to evaluate the ability of FL and T86 TDP-43s to bind the mRNAs coding for ND3 and ND6, which are transcribed from the mitochondrial genome. In agreement with Wang and co-authors (Wang *et al.* 2016), we found that the overall level of these mRNAs is not affected by TDP-43 over-expression (Figure S5) and that FL TDP-43s are able to physically bind them (Fig. 5c). This ability is minimal for T86 TDP-43, suggesting that its mitochondrial sublocalization impedes the physical contact of this truncated TDP-43 form with mitochondrial mRNAs (Fig. 6).

## Discussion

In the past few years, a potential link between mitochondrial dysfunction and defects in RNA metabolism associated with TDP-43 has been repeatedly suggested. Alteration in mitochondrial dynamics, morphology and subcellular localization were extensively described in tissues of TDP-43 transgenic mice as well as defects in mitochondrial functionality and transport into neurites of neuronal cells over-expressing wild-type or mutant TDP-43 (Shan *et al.* 2010; Xu *et al.* 2011; Hong *et al.* 2012; Lu *et al.* 2012; Wang *et al.* 2013; Stribl *et al.* 2014).

The mechanism through which a DNA-RNA-binding protein such as TDP-43 causes mitochondrial damage is unknown, but some hypotheses have been put forward (Bozzo

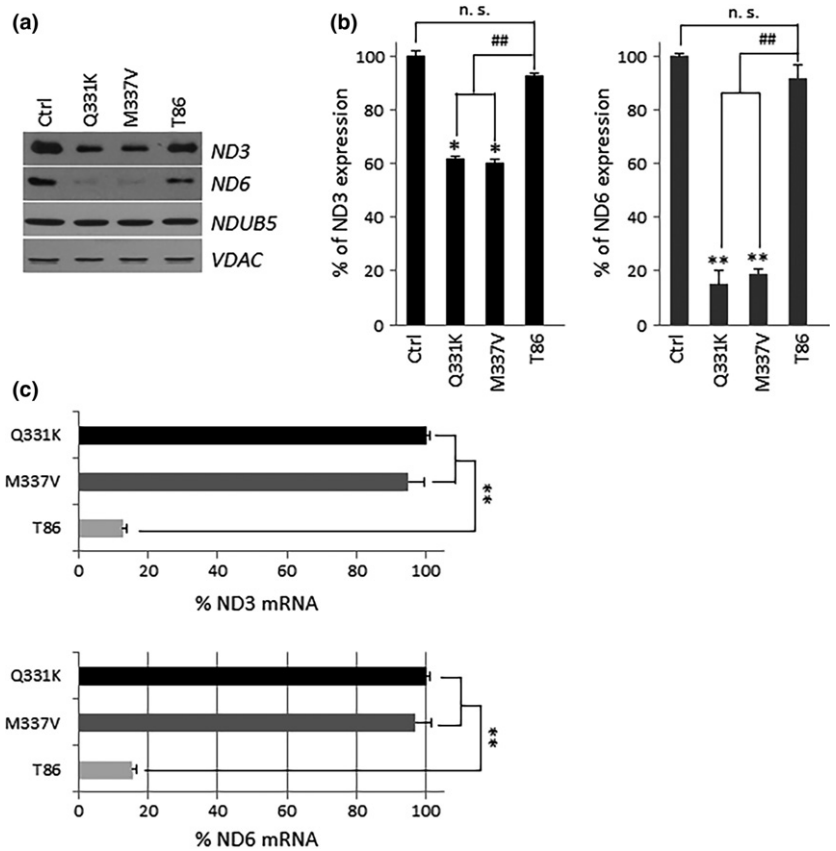


**Fig. 5** Full-length (FL) TAR DNA-binding protein 43 (TDP-43)s inhibit the expression of ND3 and ND6 via direct binding with their mitochondrial-transcribed mRNAs. (a) Western blot analysis using antibodies against ND3, ND6, NDUB5 on protein extracts from isolated mitochondria obtained from NSC-34 cells untransfected (Ctrl) and stably transfected for expression of FL (Q331K and M337V) and T86 TDP-43s. VDAC antibody was used as loading control. A representative experiment, out of three, is shown. (b) Densitometric analysis of data obtained in (a). Values significantly different from relative control (Ctrl) are indicated with $*p < 0.05$ and with $**p < 0.01$. Values significantly different from T86 with $\#\#p < 0.01$. n.s. indicates values that do not differ significantly. (c) Schematic representation of results obtained from three different experiments of RT-qPCR quantification of ND3 and ND6 mRNA in the anti-Myc immunoprecipitates from isolated mitochondria of NSC-34 cells stably transfected for expression of FL (Q331K and M337V) and T86 TDP-43s. Values significantly different from Q331K TDP-43 (arbitrarily considered 100%) are indicated with $**p < 0.01$.

*et al.* 2017). TDP-43 seems to be able to bind and exert a regulative control over transcriptional factors or proteins involved in the antioxidant defence such as superoxide dismutase 2 and catalase (Zhang *et al.* 2014). Another possibility is that mutations in TDP-43 have a direct effect on the regulation of specific mRNAs coding for proteins involved in mitochondrial physiology. This hypothesis is supported by the recent observation that ALS-related TDP-43 mutations are responsible for the alteration of the splicing pattern of nuclear-transcribed mRNAs coding for mitochondrial fission regulator-1, an IMM protein involved in mitochondrial fission (Finelli *et al.* 2015). A third possibility is that damage is induced directly (through sequestration or other unknown mechanisms) by the small fraction of the protein that localizes into these organelles. In agreement with this last hypothesis, in two seminal papers, Wang and co-authors have demonstrated that in patients and in animal and cellular models, wild-type and mutant TDP-43 bind mitochondria-transcribed messenger RNAs encoding two subunits, ND3 and ND6, of the respiratory Complex I, impairing their expression and causing Complex I disassembly. Moreover, suppression of TDP-43 mitochondrial localization abolishes wild-type and mutant TDP-43-induced mitochondrial dysfunction and neuronal loss, and improves the pathological phenotypes of transgenic mice expressing mutant TDP-43 (Wang *et al.* 2016, 2017). Both mutant and wild-type TDP-43s are localized on the matrix facing of the IMM, entering mitochondria through three putative mitochondrial localization sequences named M1, M3, M5. Wang *et al.*, proposed that M1, that is situated in the N-terminus domain, is the main responsible for the localization of TDP-43 into mitochondria, since its elimination is sufficient to inhibit the translocation of TDP-43 in this

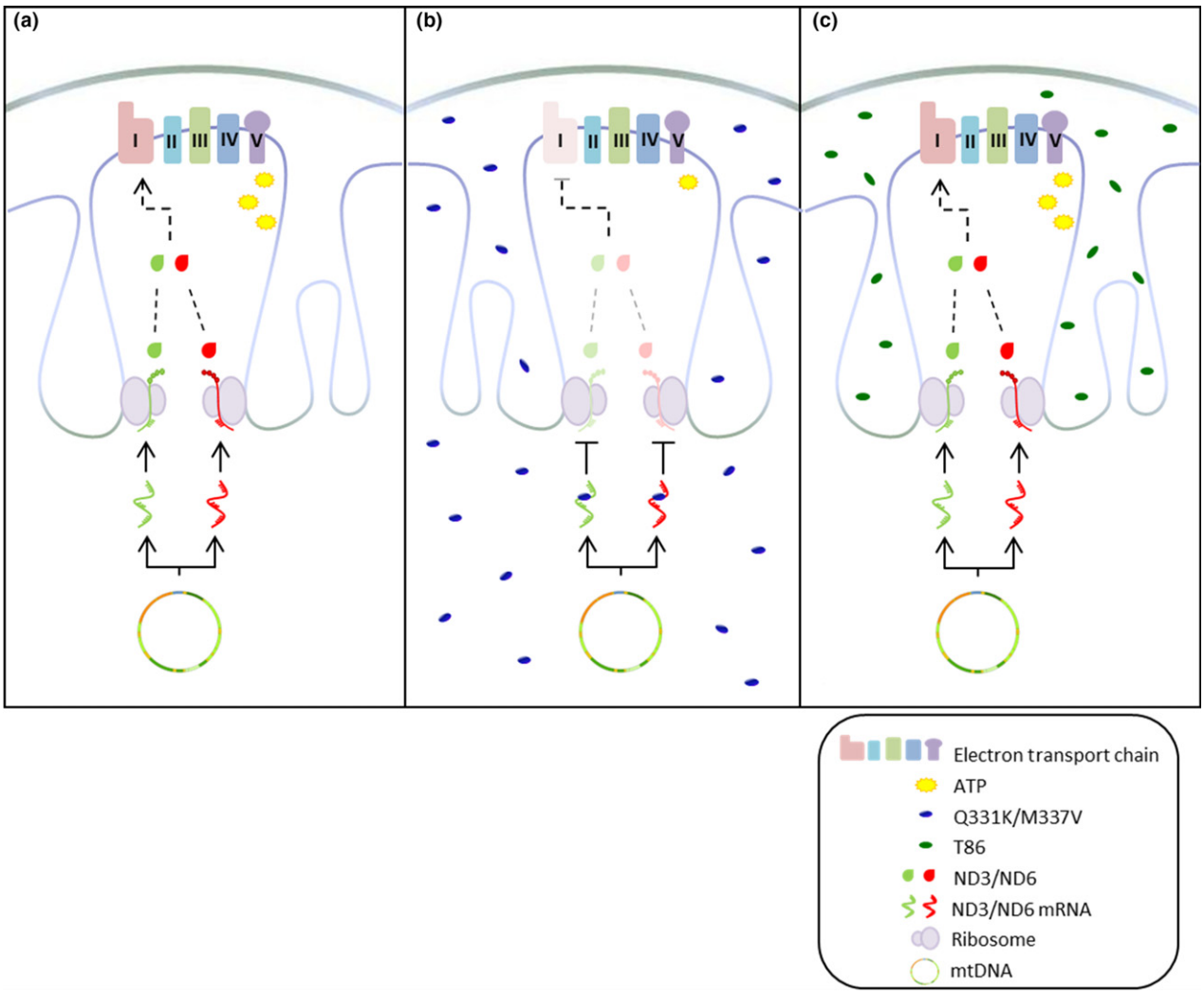


**Fig. 6** Model for TAR DNA-binding protein 43 (TDP-43)-mediated mitochondrial toxicity. (a) Control cells; (b) Full-length (FL) TDP-43s expressing cells; (c) T86 TDP-43 expressing cells. The mitochondrial localization of T86 TDP-43 is restricted to the intermembrane mitochondrial space where the protein is unable to interact with mitochondrial mRNAs, while FL TDP-43s (possessing the mitochondrial localization signal M1) are able to enter the mitochondrial matrix where they physically interact with two specific mitochondrial mRNAs (coding for two Complex I subunits, ND3 and ND6) and inhibit their translation.

cellular compartment and consequently its neuronal toxicity. Differently, Hong *et al.* (2012) reported that both 25 kDa and 35 kDa truncated TDP-43 forms (despite their lack of M1, M3 and M1 sequences respectively) localize in mitochondria in NSC-34 cells and induce activation of mitophagy even if with a lower efficacy than FLs TDP-43 (Hong *et al.* 2012).

The association of TDP-43 with mitochondria has been recently questioned by two papers (Onesto *et al.* 2016; Kawamata *et al.* 2017) reporting the absence of TDP-43 forms mitochondria. In particular, Kawamata and colleagues investigated the mitochondrial localization of both wild-type and mutant forms of TDP-43 using cellular and animal models, as well as patient-derived fibroblasts failing to find any association of these proteins with these organelles. However, with the aim to hamper any spurious association of TDP-43 with mitochondria without affecting the integrity of mitochondria and their physiologic proteome (Mishra and Mishra 2015), we used a different experimental condition and treated the purified organelles with 50 mM KCl as previously described (Ferri *et al.* 2006) (instead of 6 M KCl). In this condition and in agreement with Hong and collaborators (Hong *et al.* 2012), we found that the truncated 35kD TDP-43 form is more associated with whole mitochondria than FL TDP-43s. The mitochondrial accumulation of this truncated form, however, does not affect mitochondrial metabolism and morphology, while the little amount of FL TDP-43s localized into mitochondria matrix is enough to specifically impair Complex I activity. It is noteworthy that

the ability to affect the activity of this complex is shared by other ALS-related proteins such as mutant forms of Coiled-Coil-Helix-Coiled-Coil-Helix Domain Containing 10 and superoxide dismutase 1, outlining a common pathogenic mechanism that involves the energetic metabolism of mitochondria (Loizzo *et al.* 2010; Wang *et al.* 2016; Straub *et al.* 2017).

Our data indicate that the different behaviour in triggering mitochondrial damage between the truncated form and the FL TDP-43s lies in their different mitochondrial sublocalization in our neuronal cell lines. Indeed, we observed that the mitochondrial association of T86 TDP-43 is restricted to IMS while, in agreement with Wang and colleagues (Wang *et al.* 2016), the FLs forms enter the matrix and aberrantly interact with mRNA coding for two Complex I subunits, hampering their translation. At variance with what was observed by Wang and colleagues, we did not observe the association of mutant FL TDP-43s with the matrix face of the IMM, rather these proteins seem to be soluble into the matrix. A possible explanation is that our mitochondrial subcompartment fractionation protocol failed to preserve the RNA-mediated interaction between TDP-43 and the ribosomes docked to the inner membrane of the organelle. However, T86 TDP-43, that has both RNA-binding motifs and therefore is potentially able to bind RNA (Kitamura *et al.* 2016), does not affect Complex I activity because its restricted localization into the IMS prevents the binding with ND3 and ND6 mitochondria-transcribed mRNAs. In the light of these results, the toxicity of the truncated forms should be reconsidered. Noteworthy, that transiently expressed wild-type TDP-43 down-regulates ND-3 and ND-6 expressions suggests that, according to Wang *et al.* (2016), the wild-type form enters mitochondrial matrix interfering with ND-3 and ND6 mRNA translation similarly to mutant FL TDP-43s.

The 35kD form, lacking M1 mitochondrial localization sequence, is not able to enter mitochondrial matrix and does not affect mRNA translation into the organelle, while the 25kD form, being defective of RNA-binding motifs, is not able to bind mRNAs (Kitamura *et al.* 2016; Wei *et al.* 2017) and also lacks the M1 and M3 mitochondrial localization sequences. Thus, neuronal toxicity of both pathological truncated forms is most probably as a result of mechanisms not related to the alteration of mitochondrial metabolism. We have previously demonstrated that these shortened forms are found entirely included in oligomers when full-length TDP-43 is expressed, and that they play a central role in the generation of large cytoplasmic TDP-43 aggregates (Bozzo *et al.* 2016). The aggregation process of the truncated forms is mediated by the oxidative modification of cysteine residues, and therefore oxidative stress exacerbates the inclusion of the truncated forms into oligomers (Bozzo *et al.* 2016). Since dysfunction of Complex I is known to be the main source of cellular-free radicals production (Giachin *et al.* 2016), we propose that all the FL TDP-43s induce oxidative stress through specific alteration of Complex I and mitochondrial energetic metabolism and thus contribute to neuronal damage increasing the inclusion of the truncated forms into oligomers.

## Acknowledgments and conflict of interest disclosure

This work was supported by AriSLA (Project OligoALS to M.T.C.) and by a grant from MIUR (PRIN 2015LFPNMN to M.T.C. and to M.C.). We gratefully acknowledge Dr. Fiorella Colasuonno for technical support. The authors have no conflict of interest to declare.

All experiments were conducted in compliance with the ARRIVE guidelines.

## Supporting information

Additional supporting information may be found online in the Supporting Information section at the end of the article.

**Figure S1.** Schematic representation of the TDP-43 constructs used in this study.

**Figure S2.** (a) Western blot analysis of 20 μg of total protein extract from NSC-34 cells stable expressing WT, Q331K, M337V and T86 TDP-43 using anti-MYC and TDP-43 antibodies. β-Actin was used as loading control. (b) Western blot analysis of 20 μg of total protein extract from NSC-34 clones expressing WT TDP-43 protein, using an anti-Myc antibodies. β-Actin was used as loading control.

**Figure S3**. (a) NSC34 cells were transiently transfected with plasmids coding for the TDP-43 variants (WT, Q331K, M337V and T86) for the expression of Myc-tagged and analysed by western blot with an anti-Myc antibody. β-Actin was used as loading control. (b) Western blot analysis of mitochondrial protein extract obtained from NSC-34 cells transiently transfected (as in 'a') using anti-Myc antibody. Fractions were controlled for the presence of the mitochondrial marker VDAC, the nuclear marker HDAC1, the cytosolic marker GADPH. (c) Profile of mitochondrial stress test that measures the rate of oxygen consumption (OCR) in transfected NSC-34 viable cells (Ctrl) for the expression of WT, Q331K, M337V and T86 TDP-43s. A representative experiment on three. (d) Western blot analysis using antibodies against ND3, ND6, anti-Myc on protein extracts from isolated mitochondria obtained from NSC-34 stably transfected (as above) for expression. The VDAC antibody was used as a load control.

**Figure S4.** Expression of ND3 and ND6 mRNAs has been assessed by quantitative RT-PCR in NSC-34 cell lines expressing different TDP-43 forms.

**Table S1.** Oligonucleotides.

## References

Amador-Ortiz C., Lin W. L., Ahmed Z., Personett D., Davies P., Duara R., Graff-Radford N. R., Hutton M. L. and Dickson D. W. (2007) TDP-43 immunoreactivity in hippocampal sclerosis and Alzheimer's disease. *Ann. Neurol.* **61**, 435–445.

Arai T., Hasegawa M., Akiyama H. *et al.* (2006) TDP-43 is a component of ubiquitin-positive tau-negative inclusions in frontotemporal lobar degeneration and amyotrophic lateral sclerosis. *Biochem. Biophys. Res. Commun.* **351**, 602–611.

Ayala Y. M., De Conti L., Avendaño-Vázquez S. E. *et al.* (2011) TDP-43 regulates its mRNA levels through a negative feedback loop. *EMBO J.* **30**, 277–288.

Barmada S. J., Skibinski G., Korb E., Rao E. J., Wu J. Y. and Finkbeiner S. (2010) Cytoplasmic mislocalization of TDP-43 is toxic to neurons and enhanced by a mutation associated with familial amyotrophic lateral sclerosis. *J. Neurosci.* **30**, 639–649.

Bozzo F., Salvatori I., Iacovelli F., Mirra A., Rossi S., Cozzolino M., Falconi M., Valle C. and Carri M. T. (2016) Structural insights into the multi-determinant aggregation of TDP-43 in motor neuron-like cells. *Neurobiol. Dis.* **94**, 63–72.

Bozzo F., Mirra A. and Carri M. T. (2017) Oxidative stress and mitochondrial damage in the pathogenesis of ALS: new perspectives. *Neurosci. Lett.* **636**, 3–8.

Braun R. J., Sommer C., Carmona-Gutierrez D., Khoury C. M., Ring J., Buttner S. and Madeo F. (2011) Neurotoxic 43-kDa TAR DNA-binding protein (TDP-43) triggers mitochondrion-dependent programmed cell death in yeast. *J. Biol. Chem.* **286**, 19958–19972.

Buratti E. (2017) TDP-43 post-translational modifications in health and disease. *Expert Opin Ther Targets* **22**, 279–293.

Chen-Plotkin A. S., Lee V. M. and Trojanowski J. Q. (2010) TAR DNA-binding protein 43 in neurodegenerative disease. *Nat. Rev. Neurol.* **6**, 211–220.

Ferri A., Cozzolino M., Crosio C., Nencini M., Casciati A., Gralla E. B., Rotilio G., Valentine J. S. and Carri M. T. (2006) Familial ALS-superoxide dismutases associate with mitochondria and shift their redox potentials. *Proc Natl Acad Sci U S A* **103**, 13860–13865.

Finelli M. J., Liu K. X., Wu Y., Oliver P. L. and Davies K. E. (2015) Oxr1 improves pathogenic cellular features of ALS-associated FUS and TDP-43 mutations. *Hum. Mol. Genet.* **24**, 3529–3544.

Frezza C., Cipolat S. and Scorrano L. (2007) Organelle isolation: functional mitochondria from mouse liver, muscle and cultured fibroblasts. *Nat. Protoc.* **2**, 287–295.

Giachin G., Bouverot R., Acajjaoui S., Pantalone S. and Soler-López M. (2016) Dynamics of human mitochondrial complex I assembly: implications for neurodegenerative diseases. *Front Mol Biosci.* **3**, 43.

Hong K., Li Y., Duan W., Guo Y., Jiang H., Li W. and Li C. (2012) Full-length TDP-43 and its C-terminal fragments activate mitophagy in NSC34 cell line. *Neurosci. Lett.* **530**, 144–149.

Kawamata H., Peixoto P., Konrad C. *et al.* (2017) Mutant TDP-43 does not impair mitochondrial bioenergetics in vitro and in vivo. *Mol. Neurodegener.* **12**, 37.

Kitamura A., Nakayama Y., Shibasaki A., Taki A., Yuno S., Takeda K., Yahara M., Tanabe N. and Kinjo M. (2016) Interaction of RNA with a C-terminal fragment of the amyotrophic lateral sclerosis-associated TDP43 reduces cytotoxicity. *Sci. Rep.* **6**, 19230.

Lin W. L. and Dickson D. W. (2008) Ultrastructural localization of TDP-43 in filamentous neuronal inclusions in various neurodegenerative diseases. *Acta Neuropathol.* **116**, 205–213.

Liu-Yesucevitz L., Bilgutay A., Zhang Y. J. *et al.* (2010) Tar DNA binding protein-43 (TDP-43) associates with stress granules: analysis of cultured cells and pathological brain tissue. *PLoS ONE* **5**, e13250.

Loizzo S., Pieri M., Ferri A., Carri M. T., Zona C., Fortuna A. and Vella S. (2010) Dynamic NAD(P)H post-synaptic autofluorescence signals for the assessment of mitochondrial function in a neurodegenerative disease: monitoring the primary motor cortex of G93A mice, an amyotrophic lateral sclerosis model. *Mitochondrion* **10**, 108–114.

Lu J., Duan W., Guo Y., Jiang H., Li Z., Huang J., Hong K. and Li C. (2012) Mitochondrial dysfunction in human TDP-43 transfected NSC34 cell lines and the protective effect of dimethoxy curcumin. *Brain Res. Bull.* **89**, 185–190.

Mishra S. and Mishra R. (2015) Molecular integrity of mitochondria alters by potassium chloride. *Int J Proteomics* **2015**, 647408.

Neumann M., Sampathu D. M., Kwong L. K. *et al.* (2006) Ubiquitinated TDP-43 in frontotemporal lobar degeneration and amyotrophic lateral sclerosis. *Science* **314**, 130–133.

Onesto E., Colombrita C., Gumina V. *et al.* (2016) Gene-specific mitochondria dysfunctions in human TARDBP and C9ORF72 fibroblasts. *Acta Neuropathol Commun* **4**, 47.

Salvatori I., Valle C., Ferri A. and Carri M. T. (2017) SIRT3 and mitochondrial metabolism in neurodegenerative diseases. *Neurochem. Int.* **109**, 184–192.

Sasaki S., Takeda T., Shibata N. and Kobayashi M. (2010) Alterations in subcellular localization of TDP-43 immunoreactivity in the anterior horns in sporadic amyotrophic lateral sclerosis. *Neurosci. Lett.* **478**, 72–76.

Schwab C., Arai T., Hasegawa M., Yu S. and McGeer P. L. (2008) Colocalization of transactivation-responsive DNA-binding protein 43 and huntingtin in inclusions of Huntington disease. *J. Neuropathol. Exp. Neurol.* **67**, 1159–1165.

Shan X., Chiang P. M., Price D. L. and Wong P. C. (2010) Altered distributions of Gemini of coiled bodies and mitochondria in motor neurons of TDP-43 transgenic mice. *Proc Natl Acad Sci U S A* **107**, 16325–16330.

Stoica R., De Vos K. J., Paillusson S. *et al.* (2014) ER-mitochondria associations are regulated by the VAPB-PTPIP51 interaction and are disrupted by ALS/FTD-associated TDP-43. *Nat. Commun.* **5**, 3996.

Straub I. R., Janer A., Weraarpachai W., Zinman L., Robertson J., Rogaeva E. and Shoubridge E. A. (2017) Loss of CHCHD10-CHCHD2 complexes required for respiration underlies the pathogenicity of a CHCHD10 mutation in ALS. *Hum. Mol. Genet.* **27**, 178–189.

Stribl C., Samara A., Trumbach D. *et al.* (2014) Mitochondrial dysfunction and decrease in body weight of a transgenic knock-in mouse model for TDP-43. *J. Biol. Chem.* **289**, 10769–10784.

Tremblay C., St-Amour I., Schneider J., Bennett D. A. and Calon F. (2011) Accumulation of transactive response DNA binding protein 43 in mild cognitive impairment and Alzheimer disease. *J. Neuropathol. Exp. Neurol.* **70**, 788–798.

Valle C., Salvatori I., Gerbino V., Rossi S., Palamiuc L., Rene F. and Carri M. T. (2014) Tissue-specific deregulation of selected HDACs characterizes ALS progression in mouse models: pharmacological characterization of SIRT1 and SIRT2 pathways. *Cell Death Dis.* **5**, e1296.

Wang W., Li L., Lin W. L., Dickson D. W., Petrucelli L., Zhang T. and Wang X. (2013) The ALS disease-associated mutant TDP-43 impairs mitochondrial dynamics and function in motor neurons. *Hum. Mol. Genet.* **22**, 4706–4719.

Wang W., Wang L., Lu J. *et al.* (2016) The inhibition of TDP-43 mitochondrial localization blocks its neuronal toxicity. *Nat. Med.* **22**, 869–878.

Wang W., Arakawa H., Wang L. *et al.* (2017) Motor-coordinative and cognitive dysfunction caused by mutant TDP-43 could be reversed by inhibiting its mitochondrial localization. *Mol. Ther.* **25**, 127–139.

Wei Y., Lim L., Wang L. and Song J. (2017) ALS-causing cleavages of TDP-43 abolish its RRM2 structure and unlock CTD for enhanced aggregation and toxicity. *Biochem. Biophys. Res. Commun.* **485**, 826–831.

Xu Y. F., Zhang Y. J., Lin W. L., Cao X., Stetler C., Dickson D. W., Lewis J. and Petrucelli L. (2011) Expression of mutant TDP-43 induces neuronal dysfunction in transgenic mice. *Mol. Neurodegener.* **6**, 73.

Zhang Y. J., Xu Y. F., Dickey C. A., Buratti E., Baralle F., Bailey R., Pickering-Brown S., Dickson D. and Petrucelli L. (2007) Progranulin mediates caspase-dependent cleavage of TAR DNA binding protein-43. *J. Neurosci.* **27**, 10530–10534.

Zhang T., Baldie G., Periz G. and Wang J. (2014) RNA-processing protein TDP-43 regulates FOXO-dependent protein quality control in stress response. *PLoS Genet.* **10**, e1004693.